Active structural acoustic control of rotating machinery using piezo-based rotating inertial actuators

G. Zhao[1], N. Alujevic[1], B. Depraetere[2], G. Pinte[2], J. Swevers[1], P. Sas[1]
[1] KU Leuven, Department of Mechanical Engineering
Celestijnenlaan 300 B, B-3001, Heverlee, Belgium
e-mail: **guoying.zhao@mech.kuleuven.be**

[2] Flanders Mechatronics Technology Centre
Celestijnenlaan 300 D, B-3001, Heverlee, Belgium

Abstract

In this paper, two Piezo-Based Rotating Inertial Actuators (PBRIAs) are considered for the suppression of the structure-borne noise radiated from rotating machinery. As add-on devices, they can be directly mounted on a rotational shaft, in order to intervene as early as possible in the transfer path between disturbance and the noise radiators. A MIMO form FxLMS control algorithm is employed to generate the appropriate actuation signals, relying on a linear interpolation scheme to approximate the nonlinear secondary plants. The proposed active vibration control approach is tested on an experimental test bed comprising a rotating shaft mounted in a frame to which a noise-radiating plate is attached. The disturbance force is introduced by an electrodynamic shaker. The experimental results show that when the shaft rotates below 180 rpm, more than a 7 dB reduction can be achieved in terms of plate vibrations, along with a reduction in the same order of magnitude in terms of noise radiation.

1   Introduction

Noise radiation from structural housing in rotating machinery is a common problem in many industrial applications such as gearboxes, compressors, electric motors etc. In these cases, vibrations of rotating elements, which are transmitted though the bearings to the noise radiating surfaces such as the machine frame, are often the major noise source. In order to reduce the received noise level, techniques such as sound absorption based insulation, including encapsulation, can be used to interrupt the airborne sound transmission from the machine to the environment. These passive sound control techniques would typically be used to deal with noise at higher frequencies. At lower frequencies, where the acoustic wavelength is much larger than the maximum permissible thickness of the insulation layers, active noise control strategies can be considered instead [1]-[4]. These however become more complicated and more expensive, or alternatively less efficient, if the size of the enclosure where the sound is controlled [3] is comparatively large. Lots of error sensors and control actuators are necessary for good control performance, and in fact the total length of the wiring to connect peripheral units to the centralised controller can become a limitation [4]. In such situations it could be preferred to directly reduce the vibro-acoustic response of the noise radiating surfaces. This can be done by applying control forces on the surfaces [5], [6], [11]-[17] or isolating the transmission force to the surfaces [18]-[25]. In case forces are applied directly to the noise radiation surfaces, passive tuned mass dampers [7]-[10], inertial shakers [11]-[13], reactive actuators [14] or piezoelectric patches [15]-[17] are often employed to produce the control forces. However, this approach may become cumbersome and expensive for large and complex systems which have many radiating surfaces.

On the other hand, in the active vibration isolation approach it is attempted to block the transmitted vibrations in the structural transfer paths before they reach the noise radiating surfaces. This may yield a control system that is less complex in case there are concentrated bottlenecks in the vibration transmission

paths. With rotating machinery such concentrations typically occur in bearings that support revolving shafts. Several studies based on this approach have been published recently. Rebbechi et al. [19] proposed to integrate two pairs of magnetostrictive actuators into a double row bearing, which is mounted on the input shaft next to the input pinion, with the aim of actively isolating the vibration transmitted from the shaft to the housing. A reduction of 20-28 dB can be obtained in the housing vibration at the fundamental gear mesh frequency. Pinte et al. and Stallaert et al. [20]-[21] adopted a similar approach, but used two piezoelectric actuators instead, which are perpendicularly mounted onto one of the support bearing locations in order to limit the force transmitted from the shaft to the housing. Chen and Brennan [22] presented an inertial actuator control concept, where three magnetostrictive inertial shakers are positioned tangentially at 120° intervals on the gear body, in order to suppress the gear vibrations at the source. The above mentioned actuation concepts for the suppression of gearbox housing vibrations are theoretically compared by Guan et al. [23]. In this theoretical study, the actuation effort, control robustness and implementation costs are taken into account as the comparison criteria for four different actuation concepts. The shaft transverse vibration active control approach appeared to be the best compromise regarding the required amplitude of the control force below 500 Hz and fairly reasonable other control parameters in the higher frequency range. Some experimental validation concerning this theoretical study can be found in [24]-[25].

In this study, an axisymmetric piezo-based rotational inertial actuator, which can be installed directly on the rotating shaft as an add-on device, is proposed and studied experimentally. The benefit of this add-on approach is that the machine stiffness is not affected as is the case with for example active bearings. Another advantage is the relative ease of implementation in a practical setting as no major structural modification is required. Furthermore, the active element is not in a critical path of the machine such that a possible failure of the piezoelectric element does not necessarily affect the functionality of the machine.

One of the aims of this paper is to investigate whether or not it is feasible to suppress tonal structural borne noise/vibration by attaching PBRIAs directly onto a rotating shaft. The control strategy is based on the filtered reference least mean squares (FxLMS) algorithm [1]-[2]. Such an algorithm has been adapted in this study for the use on rotating machine applications by utilising an interpolation scheme for time varying secondary plants. The design of the PBRIA is briefly covered in Section 2, together with the experimental test bed used to evaluate its performance. The implementation of the FxLMS control algorithm is discussed next, in Section 3, followed by a presentation of the achieved results in Sections 4.

2   Design of piezo based rotational inertia shaker

Figure 1 shows the developed prototype of the piezo-based rotating inertial actuator. The idea behind the design of the PBRIA is to use a piezoelectric actuator to introduce a force between a rotating element (e.g. the shaft) and a ring-shaped mass rotating together with the shaft. By accelerating the ring-shaped mass, compensating forces can be generated on the shaft. The Piezomechanik HPSt 150/20 piezoelectric stack actuator is used. Although the piezoelectric actuator has a sufficient stroke to compensate the disturbances on the test bed, it is acknowledged that in stiff industrial applications, where excitation forces are larger, longer piezoelectric actuators with larger sections should be used to generate the required strokes. The piezoelectric actuator is preloaded by the flexures on the other side, such that it is capable of applying bi-directional (push/pull) forces. In order to avoid bending of the piezoelectric stack actuator, four Z shaped springs are foreseen at each corner, with the actuator centrally located. For the Z shaped spring, the vertical links are much shorter and, more importantly, thicker than the horizontal links such that a high rotational stiffness and a low horizontal stiffness are realized.

The actuation performance of the current design is assessed by measuring its blocked force, which is defined as the force that the actuator generates when it is constrained not to move [26]. Figure 2 shows the set-up made for the measurements on the blocked force. The inner ring of the PBRIA is fixed to a heavy block mass through an impedance header (*PCB 288D01*) which is used to measure the force generated by the PBRIA projected in the vertical direction. A *SCADAS III* system running *LMS Test.lab* is used to measure the frequency response function (FRF) of the transfer function between the voltage applied to the

piezoelectric actuator and the generated force. Four accelerometers are positioned around the PBRIA to access the modal information of the PBRIA.
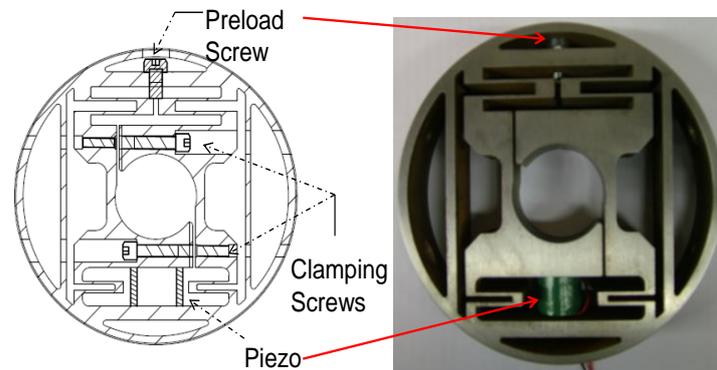

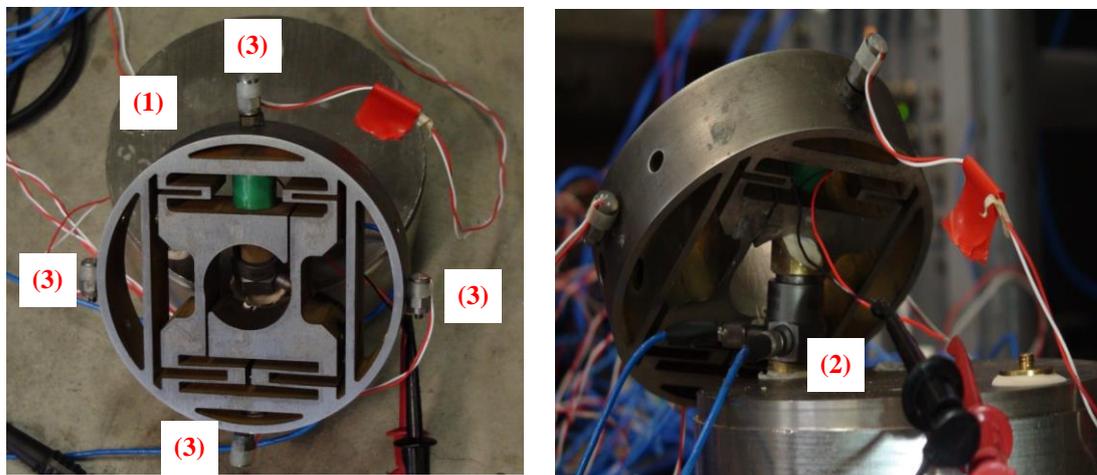Figure 1: The developed piezo-based rotating inertial shaker.

Figure 2: The measurement set-up for the blocked force: (1) base mass; (2) impedance header; (3) 1D accelerometers.

The blocked force response function is measured in the frequency range 0-2 kHz, as shown in Figure 3. In general, the maximum of the response function occurs at the fundamental resonance frequency, which is about 1300 Hz. Besides this peak, a sequence of peaks and dips are presented in the frequency ranges: 1) between 500 Hz and 700 Hz and 2) between 1400 and 1600 Hz in the measured FRF, which are due to the dynamics of the measurement set-up. For the frequencies below the fundamental frequency, the magnitude response reduces and the phase response tends to be 180°, which indicates that the blocked force at the inner ring of the PBRIA is out of phase with the driving voltage signal. Around the fundamental resonance frequency, the phase of the blocked force FRF undergoes an 180° phase–lag such that the blocked force is in phase with the driving signal at higher frequencies and the magnitude response is approximately flat up to 2 kHz. It is also of interest to note that the control force which can be applied by the PBRIA only starts to be significant when the frequency is above 200 Hz.

Therefore, the fundamental resonant frequency of the PBRIA should be carefully designed, which ideally needs to be near or less than the excitation frequency in order to have a constant and sufficient force excitation for low frequencies, see for example [27] where collocated control with direct velocity feedback has been considered. The proposed PBRIA utilizes a piezoelectric stack actuator which yields a high piezoelectric coupling coefficient (d_{33} piezoelectric effect) but also associates a high fundamental resonance frequency around 1300 Hz. This high resonance frequency of the PBRIA may preclude its application in the low frequency range. In order to lower the resonant frequency of the PBRIA, piezoelectric beams instead of piezoelectric stacks could be used in conjunction with bending beams to accelerate the outer ring mass with a d_{31} piezoelectric effect, see for example [10]. However, one should

bear in mind that the piezoelectric coupling coefficient for the d_{31} mode is reported to be approximately 2 times smaller than the d_{33} mode [28], which means it may consume more energy to exert the same excitation level. In addition, the fundamental resonance frequency of the PBRIA should be much larger than the rotating speed in order to maintain its functionality as an inertial actuator. Therefore, the actuating mechanism of choice for a PBRIA has to combine the above three considerations. The developed PBRIA has been tested to be able to excite most structural vibration modes of the test bed (will be introduced in the following paragraph) in the frequency range of interest [29], which indicates the PBRIA has control authority over the concerned frequency range.
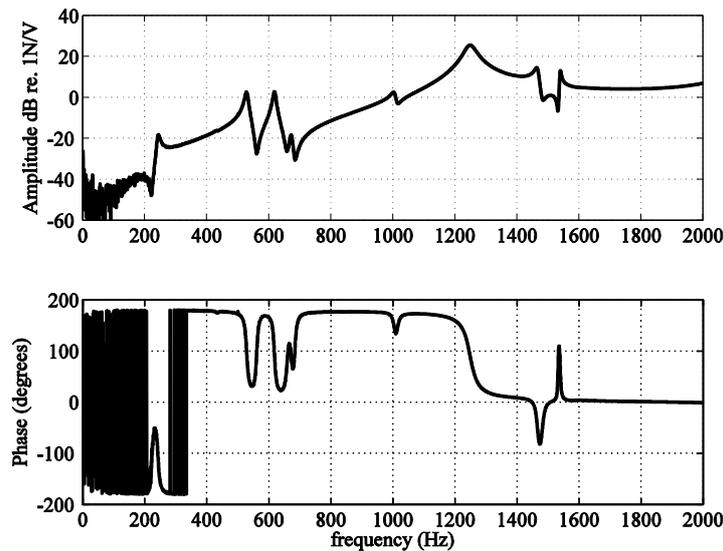

Figure 3: The measured blocked force response.

A representative set-up for rotating machinery is constructed in order to demonstrate the feasibility of the proposed active vibration control approach, which is shown in Figure 4. In this test bed, a motor drives a shaft, which is supported in a frame by a cylindrical bearing at one side and a double angular contact ball bearing at the other side. This latter bearing is mounted in a ring-shaped module in which two piezoelectric sensors are installed to measure the transmitted forces between the shaft and the frame. Close to this bearing, two PBRIAs are perpendicularly installed on the shaft such that control forces can be generated in all directions. In order to transmit control signals from a non-rotating control source, a slip ring is equipped and mounted on the shaft close to the PBRIAs to provide electrical connections to the non-rotating controller

A number of sensors are installed on and around the test bed to demonstrate the performance of the proposed control approach. The layout of the sensor configuration is shown in Figure 5, where two accelerometers are used to measure the structural vibrations, one microphone is used to register the noise level in front of the plate at a distance of approximately 30 cm and one force gauge placed between the bearing close to the PBRIA and the frame is used to record the transmission force. For the accelerometers, one of them is placed on the frame measuring vibrations in x and y axes, while the other one is mounted in the middle of the plate measuring only vibrations in x axis. The x and y axes represent the directions that are parallel and perpendicular to the disturbance line of action, as indicated in Figure 5. Hereafter, x direction refers to as the horizontal direction and y direction refers to as the vertical direction. The frame vibrations in the y axis (the vertical frame acceleration) and plate vibrations in the x axis (the horizontal plate acceleration) are chosen as the error signals for the active controller in the experiments of this study.
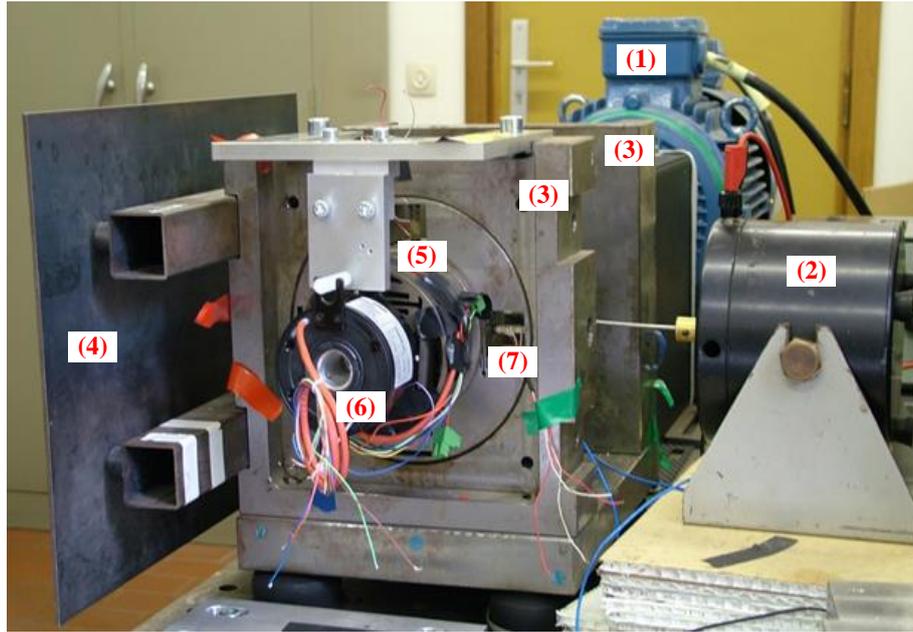
Figure 4: The experimental set-up of the test bed: (1) Motor; (2) Disturbance shaker; (3) Frame; (4) Noise radiating plate; (5) PBRIAs; (6) Slip ring; (7) Force sensor.
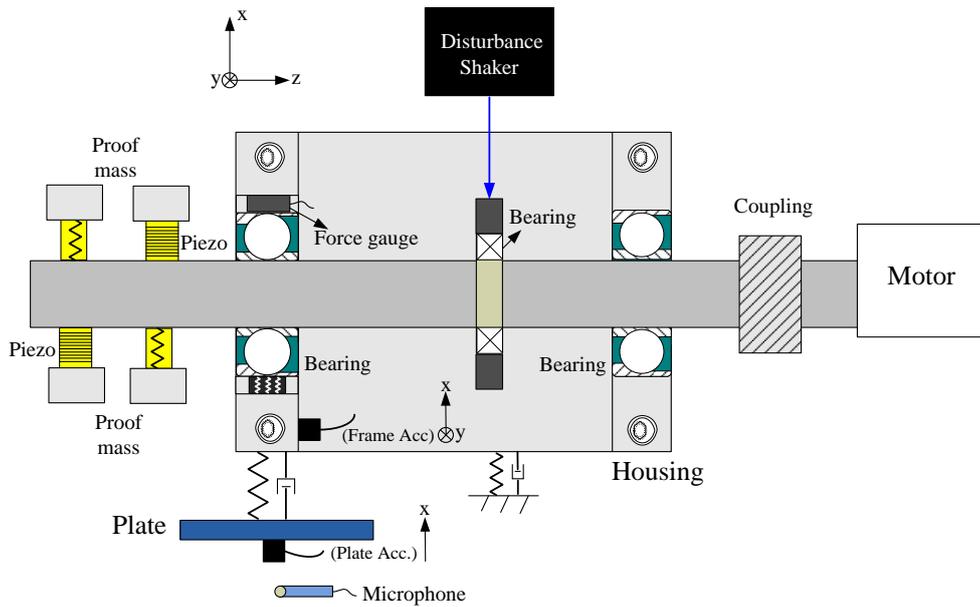

Figure 5: A cross-sectional view of the experimental set-up with all measurements

3   FxLMS adaptive controller

In this section, the FxLMS control algorithm is briefly reviewed. Its block diagram is shown in Figure 6. The core of the control scheme is an adaptive digital filter, which is usually implemented by a finite impulse response filter (FIR), denoted as $W(k)$. The coefficients of $W(k)$ are updated so that the mean square error (MSE) of a chosen error signal $e(k)$, $E\left[e^2(k)\right]$ is minimized. This is usually done by using

the steepest decent method. Using the instant squared error signal $e^2(k)$ to estimate the MSE, the well-known least mean square (LMS) algorithm for updating the coefficients of $W(k)$ is derived:

$$W(k+1) = \beta W(k) + \mu r(k) e(k) \qquad (1)$$

where μ is the convergence coefficient, β is the power constraint with $0 < \beta \leq 1$, $e(k)$ is the instantaneous error, i.e., the difference between the disturbance signal $d(k)$ and the secondary plant ($S(q)$) output $y(k)$, and $r(k)$ is the filtered reference signal which is the convolution of the reference $x(k)$ and the estimated secondary plant $\bar{S}(q)$. Generally, the parameter μ should be as large as possible without compromising the stability of the system. A suitable value of control effort constrain β should be introduced to prevent unconstrained weight overflow and limit the output power to avoid nonlinear distortion [2]. If the parameter β is set to other value than 1, the FxLMS algorithm becomes the leaky FxLMS algorithm.
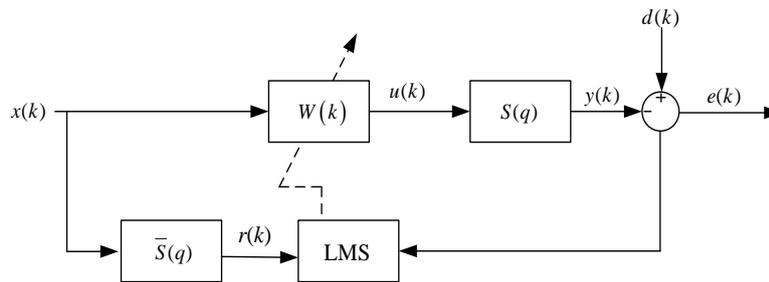

Figure 6: The block diagram of the FxLMS algorithm

Depending on the availability of the reference signal, the FxLMS algorithm can be used to control both broadband and narrowband disturbances. Considering the rotating machinery application, this study focuses on suppressing tonal disturbances and thereby the periodic filtered-X LMS algorithm is implemented and a sinusoidal signal of the same frequency of the disturbance is used as the reference signal. In such a case, the algorithm becomes an adaptive notch filter [30]-[32]. If the aim is to suppress multiple tones at the fundamental frequency and several harmonics, the reference signal can be composed by a rectangular wave with a period equal to the inverse of the fundamental frequency of the disturbance or simply the sum of all the considered sinusoids [33]. Since two PBRIAs are used in the experiments, the MIMO form of the FxLMS algorithm is investigated. Here, the controlled plants are constructed between the driving signals to the two PBRIAs and the outputs of the two accelerometers measuring the horizontal plate vibrations and the vertical frame vibrations. Although the main focus of this study is on suppressing the noise radiation from the plate, only one accelerometer placed on the plate is in principle enough for the control purpose. The other error sensor is chosen so that the test bed is not seriously influenced in the vertical direction due to the control action. As mentioned earlier, the chosen error sensors are mounted on the fixed parts of the test bed whereas the piezoelectric actuators are rotating together with the shaft. This means that the constructed secondary plants are continually changing with respect to the shaft rotational position, which in other words indicates the secondary plants are time varying.

A linear interpolation method is proposed to estimate the time varying secondary plants. The idea is to measure the secondary plants offline at several points in one revolution and estimate the rest by linearly interpolating between two adjacent known plants (the seed plants). As the secondary plants are modelled by FIR filters, the interpolation can be made directly on the coefficients of the FIR filters. If otherwise IIR (infinite impulse response) filters are used, the interpolation would best be implemented on the outputs of the IIR filters. In practical applications, since the FxLMS algorithm is fairly robust against plant modelling errors [34], it could be expected that the algorithm remains stable as long as the number of the seed plant is large enough such that the phase difference between the plant and the plant model does not exceed $90°$.

Finally, the flowchart of the employed MIMO form periodic FxLMS algorithm is depicted in Figure 7, where the various symbols have the following meanings: $x(k)$ represents the reference signal which is presumed to be a sinewave and after undergoing a 90° phase shift, giving the other reference signal $x'(k)$; $W_1(q)$ and $W_2(q)$ are the two adaptive FIR filters, each of them is composed by two filter coefficients $w_{i,j}(q)$, $i,j \in [1,2]$; $y_1(n)$ and $y_2(n)$ are the driving signals for the two PBRIAs; $e_1(n)$ and $e_2(n)$ are the error signals measured by the error sensors; $y_{d1}(n)$ and $y_{d2}(n)$ are the disturbance sources measured by the error sensors; $[S_{11}(q)]_\theta$ and $[S_{21}(q)]_\theta$ are the secondary paths from $y_1(n)$ to the two error sensors at θ degrees; $[S_{12}(q)]_\theta$ and $[S_{22}(q)]_\theta$ are the secondary paths from $y_2(n)$ to the two error sensors; $[\overline{S_{i,j}}(q)]_\theta$ is the estimate of the secondary plant for $[S_{i,j}(q)]_\theta$, $i,j \in [1,2]$. The cost function for updating the controller coefficients is the sum of the two squared error signals.
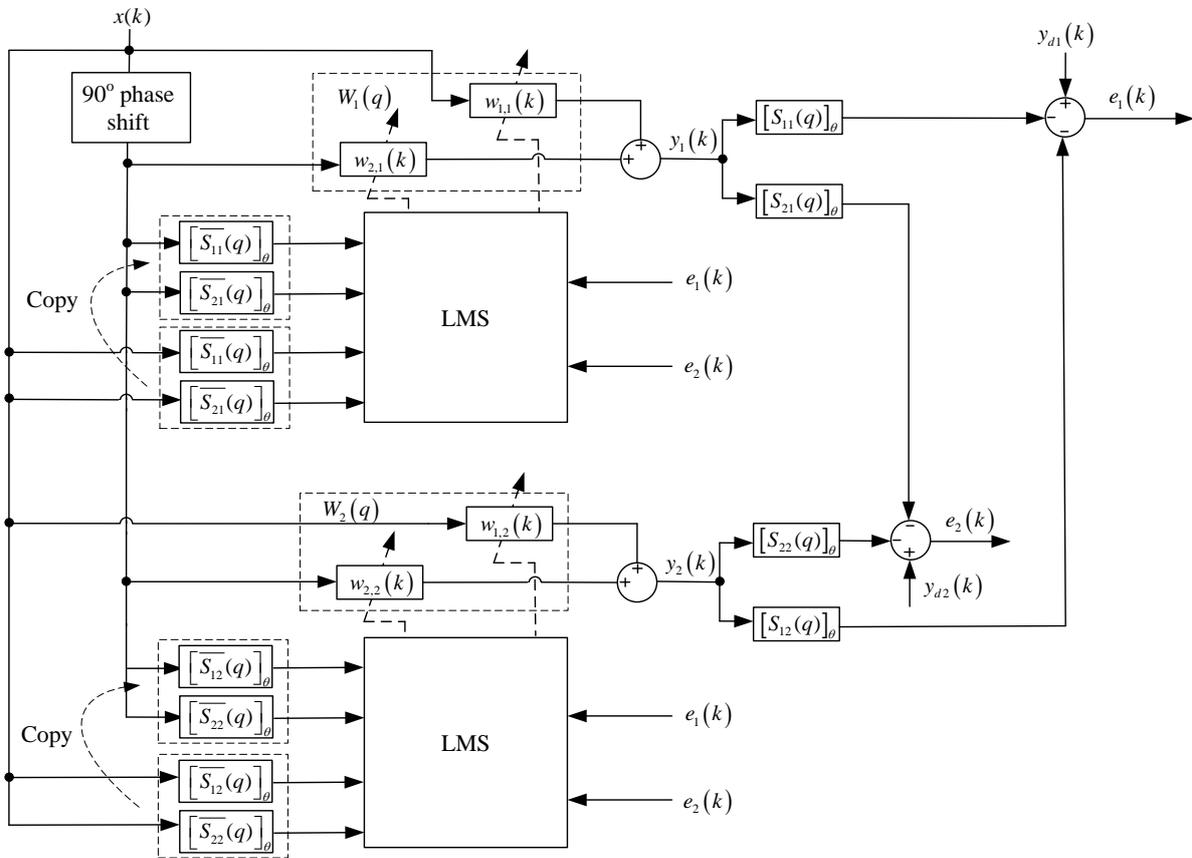

Figure 7: The flowchart of the MIMO form of the FxLMS control algorithm

4   Experimental validation

The purpose of the experiments in this section is to examine the performance of actively controlled PBRIAs in the test bed presented in the section 2. Prior to describing the results obtained, some system parameters are defined first. During the experimental study, the measured signals are recorded by a dSpace DS 2004 A/D acquiring board at a sampling frequency of 2.5 kHz. All the signals fed into the control board are filtered by a low pass filter with a 1k Hz cut-off frequency. The FxLMS controller is updated at a sampling frequency of 20 kHz. An encoder with a resolution of 1024 pulses per revolution is utilized to measure the rotational position of the shaft, the signals from which are then processed by the dSpace control broad 3001 to calculate the instant angular position. As described earlier, the horizontal

acceleration of the plate and the vertical acceleration of the frame are taken as the error signals. The disturbance is provided by the electrodynamic shaker, which can execute dynamic forces on the shaft. The electrodynamic shaker is driven by a sinusoidal signal at 371 Hz throughout the study. This frequency corresponds to one of the resonances of the sound radiating plate. The whole control scheme is implemented in the Matlab Simulink environment and then downloaded to the processor of a dSpace 1006 system. The sine wave sent to the disturbance shaker is directly taken as the reference signal for the FxLMS controller in the Simulink model. In such a case, a perfect correlation between the reference and the disturbance is assumed. In real-life applications, a tacho signal, which provides information concerning the disturbance frequency, is always taken as the reference signal. This signal can be acquired for example from an optical sensor measuring the rotational motor speed. In order to assure an adequate level of coherence between the reference and disturbance signals, the measured pulse train can be fed into a frequency estimator to estimate the instant rotating speed [24].

4.1   Secondary plant modelling and identification

The secondary plants are modelled by FIR filters, which can be estimated off-line with an LMS adaptive algorithm [2]. The process consists of exciting the secondary path with a sine wave and in the meanwhile providing the same signal as the reference to a conventional LMS algorithm. After the convergence of the algorithm, the controller coefficients will then resemble the secondary path impulse response. Since only a single frequency is considered, an FIR filter with only 2 coefficients is sufficient. By repeating this at multiple frequencies, the FIR filter coefficients for the secondary plants at all relevant frequencies can be inserted as a lookup table as a function of the disturbance frequency. An alternative is to measure the FRFs of the secondary paths in a broad frequency band, from which the FIR coefficients at one frequency can also be derived.

As mentioned above, the constructed secondary plants are angular position dependent and an interpolation scheme is needed. Here, each secondary plant is identified at 32 angular positions in one revolution. The 0˚ position is defined when piezoelectric actuator of PBRIA 1, as shown in Figure 4, is in parallel to the disturbance. Figure 8 (a) and (b) show the amplitude and phase of the secondary-plant FRFs between the voltages to the piezoelectric actuators and the measured plate vibrations at 371 Hz, while Figure 8 (c) and (d) present the FRFs of the other two secondary-plants between the voltages to the piezoelectric actuators and the measured vertical frame vibrations. As can be seen, the four plants vary with respect to the angular positions, where the crests and troughs of the curves are located at these positions when the actuation direction of the PBRIA is parallel and perpendicular to the direction of the sensors.

In the following sections, the performance of the developed controller is demonstrated in two conditions. Firstly, the shaft is not rotating. The experiments are concerned with the effect of the controller to suppress the response of different parts of the test bed. In the second step, the focus is on examining the effect of the controller over a selected range of operating speeds.
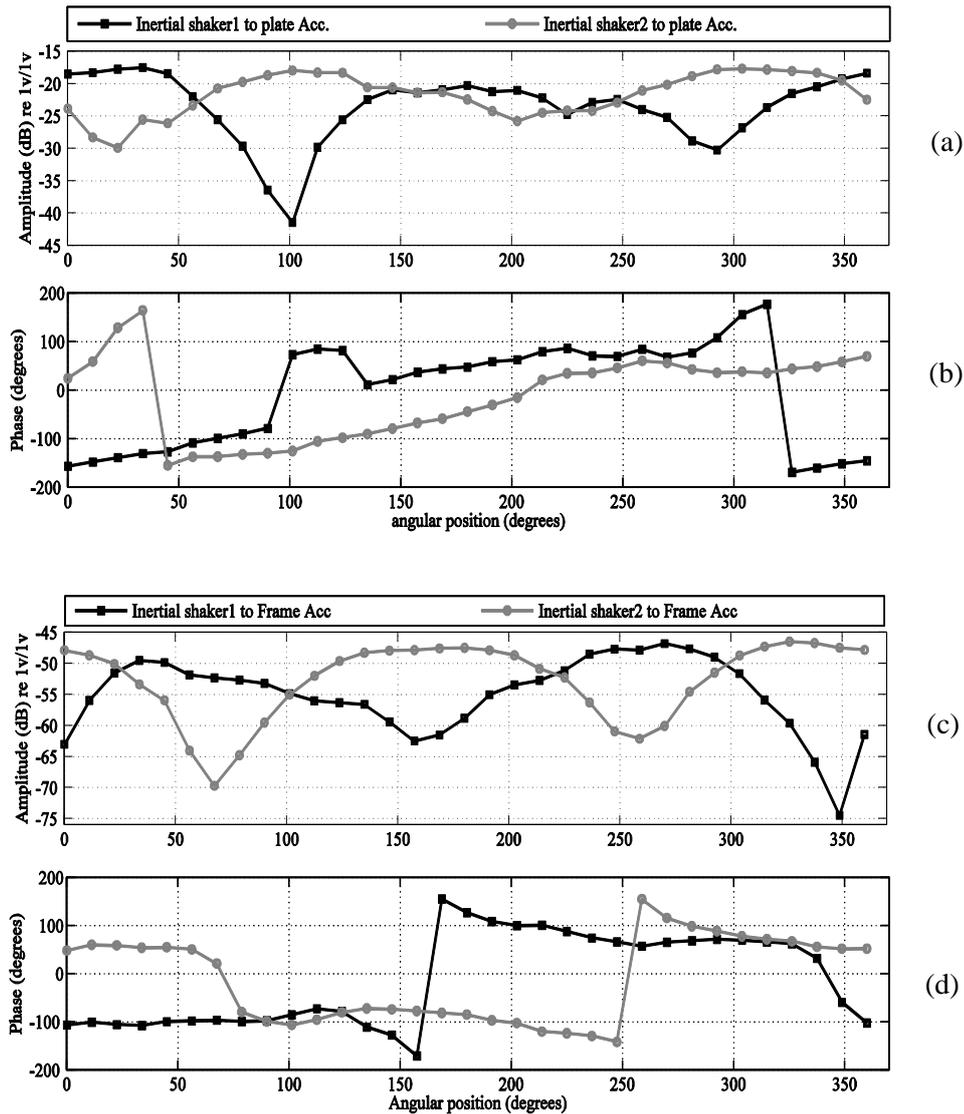
Figure 8: FRFs of the secondary plants at the 32 angular positions: (a) and (b), the amplitude and the phase of the FRFs between PBRIAs 1 and 2 to the horizontal plate vibration; (c) and (d), the amplitude and the phase of the FRFs between PBRIAs 1 and 2 to the vertical frame vibration.

4.2 Non-rotating tests

The potential of the proposed actively controlled PBRIAs is first illustrated when the shaft is not rotating and fixed at $0°$ position. The convergence rate μ is set to 0.3 which is about half of the critical value after which the system becomes unstable. The leakage factor β is set to 0 which means no power constraint is considered in this case. In Figure 9 (a) and (b), the time histories of the two error signals are presented, which are the horizontal plate acceleration and the vertical frame acceleration respectively. First, up to $t = 5$ s, the controller is inactivated and later on it is activated. It can be seen that after convergence the accelerations have decreased dramatically, with reductions of 45 dB and 31 dB respectively. The convergence period takes approximately 0.1 s and 20 s, and thus differs strongly for both. For the MIMO FxLMS control algorithm, the speed of convergence is mainly determined by two factors, which are the initial excitation levels and the spatial eigenvalues of the secondary plants matrix [3]. Here, the chosen frequency of 371 Hz coincides with one of plate resonances so that the response picked up by the accelerometer on the plate is about 10 times larger than the one measuring the vertical vibration level of the frame at this frequency, which already partially explains why the convergence for the plate

accelerations is much faster. Besides this, the spatial eigenvalue corresponding to the plate vibrations is calculated to be much larger, which can be derived from the matrix M composed by the four identified plants at 0° position in Figure 8:

$$M = \begin{bmatrix} \left[\overline{S_{1,1}}(q)\right]_0 & \left[\overline{S_{2,1}}(q)\right]_0 \\ \left[\overline{S_{1,2}}(q)\right]_0 & \left[\overline{S_{2,2}}(q)\right]_0 \end{bmatrix} \tag{2}$$

Therefore, it is reasonable to obtain the difference of the convergence speed. In order to improve or equalize the convergence speeds, a more detailed analysis is needed to alter the cost function or determine the optimal positioning of the error sensors, which is beyond the scope of this study.

Figure 9 (c), (d) and (e) plot the radiated noise, horizontal frame acceleration and the transmitted force respectively. From these, it can be seen that a reduction of the error signals also leads to a reduction in the audible noise, the transmitted force and the frame vibrations. Thus, a global response reduction is obtained, primarily because the response of the measured points is dominated by the plate mode. However, there are some residues for the transmitted force and the frame vibration in the horizontal direction (the residues for the other three signals are caused by the sensor noises), which might be attributed to the locations of the chosen error signals. In order to enhance the performance of the control approach, additional sensors can be taken as error sensors. As the FxLMS algorithm only guarantees reductions at the error sensors, the location of the PBRIAs should also be considered carefully, and they should ideally be placed as close as possible to the disturbance such that they excite the structure in the same manner as the disturbance.
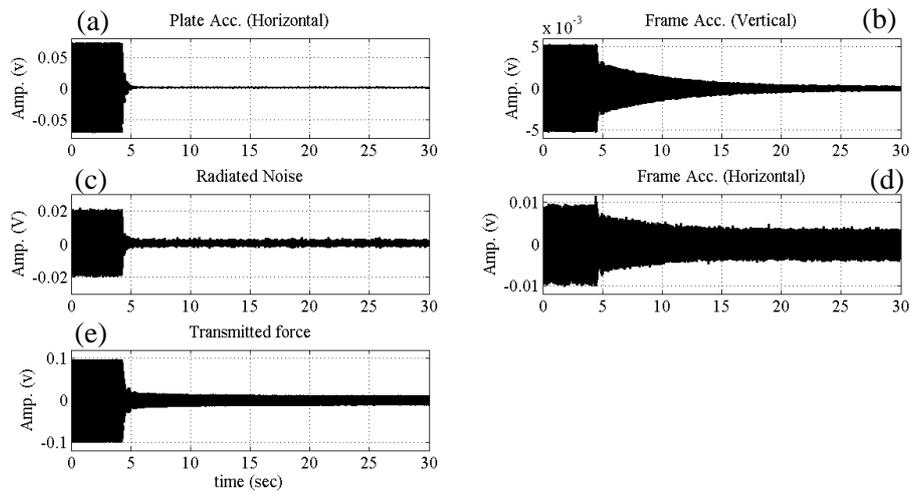

Figure 9: The control effect on (a) plate vibrations, (b) vertical frame vibrations, (c) radiated noise, (d) horizontal frame vibrations and (e) transmitted force

4.3   Rotating tests

In this subsection, experiments with the proposed PBRIAs are performed when the shaft is rotating at 60, 120 and 180 rpm respectively. The aim here is to investigate the influence of the rotating speed to the proposed control approach.

The controller filter coefficients are updated using the FxLMS algorithm. The convergence rate μ is set to 0.7 and the leaky factor β is set to 0.995. Here, certain power constraint is introduced, which is essential for the current MIMO control case where the plant matrix is nearly ill-conditioned. By doing it, unreasonable values of control effort are prevented. An additional benefit is to reduce the risk of instability and speed up the convergence of the insignificant errors [2]. Figure 10 (a) shows the measured plate vibrations at the rotating speed of 60 rpm, 120 rpm and 180 rpm (from top to bottom), first with the

developed controller deactivated, then activated and again deactivated. It can be seen that the residue level drastically increases with an increase of the rotating speed, which indicates that the control effectiveness might further degrade as the shaft operates faster. In order to further analyze these results, the achieved reductions are plotted as a function of the rotational position of the shaft. To do so, the time domain signals of the first two segments (deactivated and activated) are synchronized with the rotating speed signal measured by the encoder, and the reductions are calculated in an interval of 10°. The resultant reductions are shown in the angular domain in Figure 10 (b), where the average reductions during the different revolutions are represented by the dot-line and the variations by the error bars. As it is shown, the trend of the averaged reductions also shows the performance loss increases as the rotating speed increases. Next, the first two segments of the time domain signals in each case are projected into the frequency domain, as shown in Figure 11 (a). The achieved reductions are presented in Figure 11 (b), evaluated at the disturbance frequency itself and three pairs of rotating speed harmonics away from it. Here also, the achieved reductions at the excitation frequency reduce as the speed goes up. The main reason for the loss of the performance is that the faster change on the secondary plants makes it more challenging for the controller to follow and adapt to these changes but gets less and less time to do so. Additionally, the non-perfect estimation of the secondary plants and their nonlinearities, which means the secondary plants might vary in terms of the rotating speed, also contribute to the control effectiveness loss.
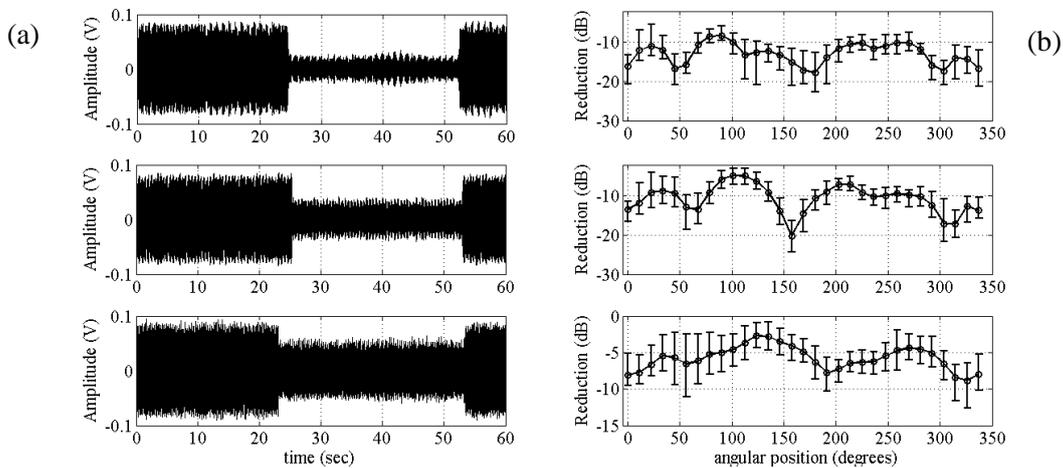

Figure 10: (a) The control effect on the plate vibrations when the shaft rotates at, from top to bottom, 60 rpm, 120 rpm and 180 rpm in the time domain; (b) The resultant reductions in the angular domain.
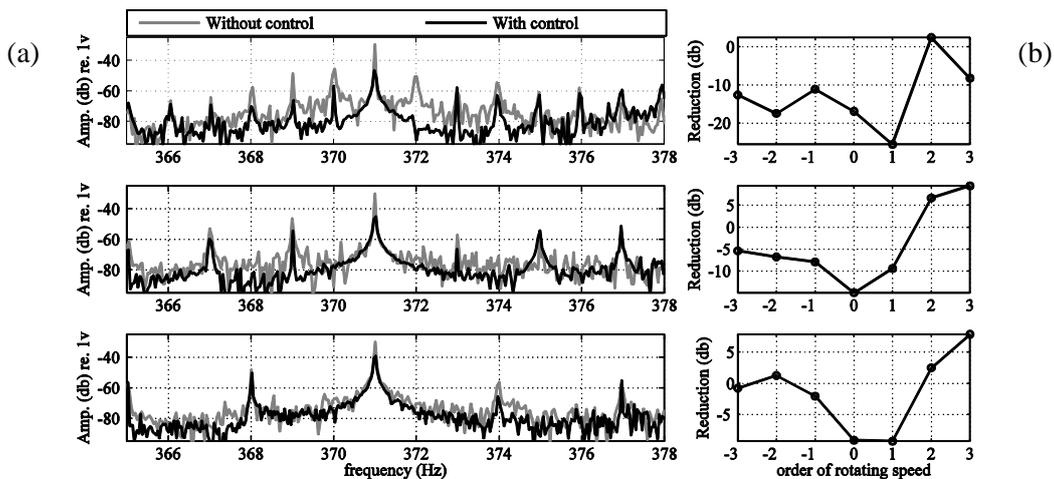

Figure 11: (a) Comparison of the plate vibrations in the frequency domain, without control and with control when the shaft rotates at, from top to bottom, 60 rpm, 120 rpm and 180 rpm; (b) the resultant reductions at the exciting frequency itself and three pairs of the rotating speed harmonics away from it.

Next, the performance for the vertical frame vibrations is also examined, as shown Figure 12 and Figure 13. Compared to the plate vibrations, the control effectiveness has now completely disappeared and amplifications are even observed at higher rotating speed. This is mainly because the convergence speed of the vertical frame vibration is much less than the one of the plate vibration such that the initial transient of the coefficients are mainly determined by the plate vibration. With the increase of the rotating speed, the performance loss on the plate vibrations, as shown in Figure 10 and Figure 11, thus leads to the poor control effectiveness on the vertical frame vibrations. Since the emphasis in the study is on the plate vibrations, the behavior of the vertical frame acceleration is to be expected. Nevertheless, the proposed active controlled PBRIAs can work effectively in a low running speed condition.
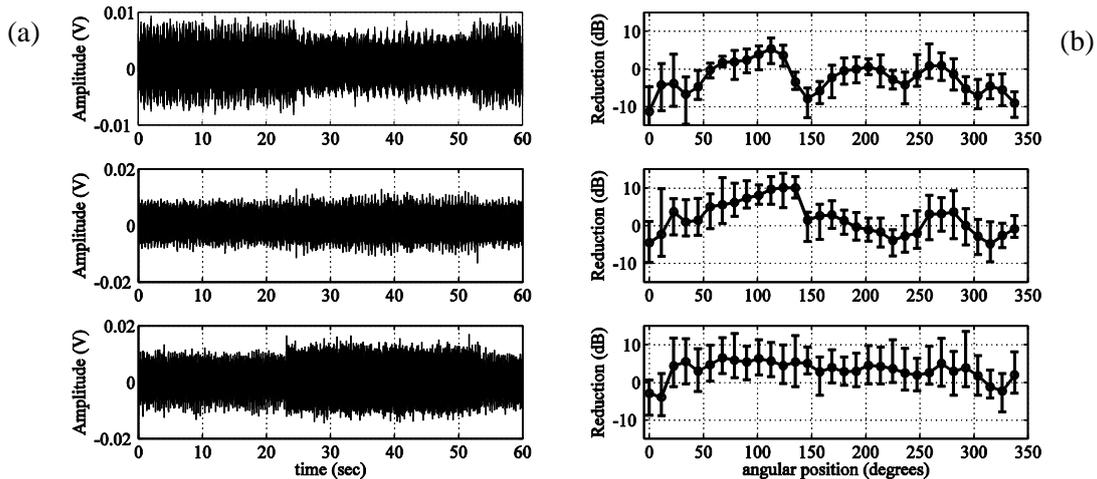

Figure 12: (a) The control effect on the vertical frame vibrations when the shaft rotates at 60 rpm, 120 rpm and 180 rpm in the time domain; (b) The resultant reductions in the angular domain.
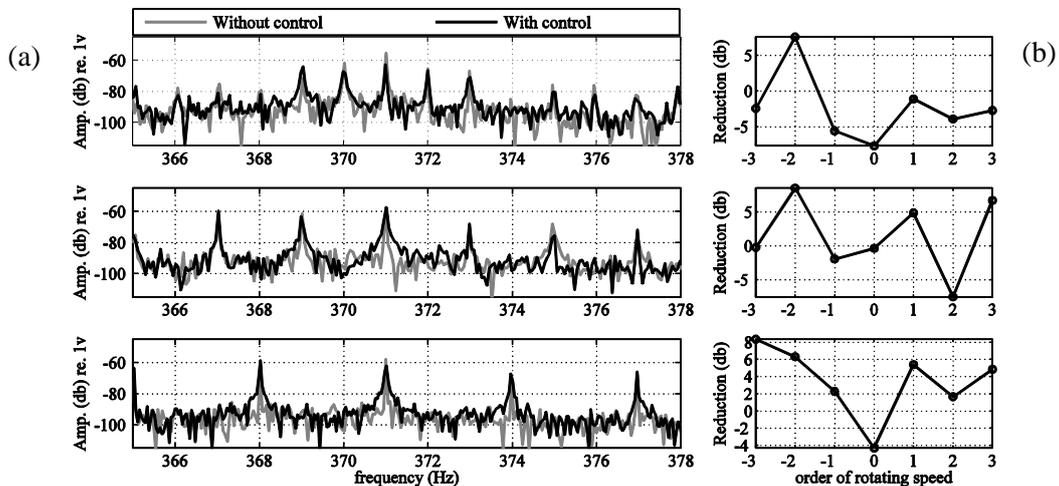

Figure 13: (a) Comparison of the vertical frame vibrations in the frequency domain, without control and with control when the shaft rotates at, from top to bottom, 60 rpm, 120 rpm and 180 rpm; (b) the resultant reductions at the exciting frequency itself and three pairs of the rotating speed harmonics away from it.

5   Conclusion

This paper discusses a novel control concept for suppressing rotating machinery radiating noise, which is to use PBRIAs that rotate together with the machinery to actively control the effects of disturbance forces transmitted to the structure housing. A MIMO form of the FxLMS algorithm is applied to control the plate vibrations and the frame vibrations. In order to account for the time varying effects of the rotating

PBRIAs, a linear interpolation scheme is proposed to model the time varying secondary plants. The design and control approach have been validated on an experimental test bed. It has been shown that more than 7 dB reductions in the plate vibrations can be achieved when the shaft rotates below 180 rpm, with the resulting reduction of acoustic noise in the same order of magnitude. These results demonstrate the technical feasibility of using the considered PBRIAs for suppressing structure borne noise of rotating machinery for applications with a low running speed. Once the speeds become high however, the controller can have difficulties following and adapting fast enough. Additionally, the non-perfect estimation of the secondary plants and their nonlinearities are more pronounced. Therefore, future studies will aim at improving the performance of the active vibration control approach for higher rotating speeds, as well as gaining a better understanding of the limitations of the followed approach.

Acknowledgements

References

[1]   P.A. Nelson, S.J. Elliott, *Active control of Sound*, Academic Press, New York, 1992

[2]   S.M. Kuo, D.R. Morgan, *Active Noise Control Systems: Algorithms and DSP Implementation*, Wiley, New York, 1996.

[3]   S.J. Elliott, C.C. Boucher and P.A. Nelson, *The behaviour of a multiple channel active control system*, IEEE transactions on Signal Processing (1992), Vol. 40(5), 1041-1052.

[4]   S. J. Elliott, P. A. Nelson, I. M. Stothers. And C. C. Boucher, *Inflight experiments on the active control of propeller-induced cabin noise*, Journal of Sound and Vibration, vol. 140. pp. 219-238, 1990.

[5]   W. Dehandschutter, *The reduction of structure-borne noise by active control of vibration*, PhD thesis, KU Leuven University, Leuven, Belgium (1997).

[6]   G. Pinte, *Active Control of Repetitive Impact Noise*, PhD thesis, KU Leuven University, Leuven, Belgium. (2007).

[7]   Den Hartog, J. P., *Mechanical Vibrations*, McGraw-Hill Book Co., New York, (1934.)

[8]   J. B. Hunt, *Dynamic Vibration Absorbers*, London: Mechanical Engineering Publications Ltd. (1979).

[9]   D. J. Inman, *Engineering Vibration*, Prentice-Hall, New York (1994).

[10]   N. Alujevic, I. Tomac and P. Gardonio, *Tunable vibration absorber using acceleration and displacement feedback*, Journal of Sound and Vibration (2012) 331(12), 2713-2728.

[11]   C. Paulitsch, P. Gardonio, S. J. Elliott, P. Sas, and R. Boonen, *Design of a Lightweight, Electrodynamic, Inertial Actuator with Integrated Velocity Sensor for Active Vibration Control of a Thin Lightly-Damped Panel*. International Conference on Noise and Vibration Engineering (ISMA), Katholieke Universiteit Leuven, Belgium, 20-23 September 2004.

[12]   C. Paulitsch, P. Gardonio, S.J. Elliott, *Active vibration control using an inertial actuator with internal damping*, Journal of the Acoustical Society of America 119 (2006) 2131–2140.

[13] N. Alujevic, G. Zhao, B. Depraetere, P. Sas, B. Pluymers and W. Desmet, $\mathcal{H}_2$ optimal *vibration control using inertial actuators and a comparison with tuned mass dampers*, Journal of Sound and Vibration (2014), 333(18), 4073-4083.

[14] N. Alujevic, P. Gardonio, and K. D. Frampton, *Smart double panel for the sound radiation control: blended velocity feedback*. AIAA Journal, vol. 49. No. 6 (2011), pp. 1123-1134.

[15] Z. Qiu, X. Zhang, H. Wu and H. Zhang, *Optimal placement and active vibration control for piezoelectric smart flexible cantilever plate*, Journal of Sound and Vibration (2007) 301, 521-543.

[16] E. Crawley and J. de Luis, *Use of piezoelectric actuators as elements of intelligent structures*, AIAA Journal 25 (1987) 1373-1385.

[17] C. R. Fuller, S. J. Elliott and P. A. Nelson, Active control of Vibration, Academic Press, San Diego, CA92101, 1986.

[18] T. J. Sutton, S. J. Elliott, M. J. Brennan, K. H. Heron and D. A. C. Jessop, *Active Isolation of Multiple Structural Waves on a Helicopter Gearbox Support Strut*, Journal of Sound and Vibration (1997) 205(1), 81-101.

[19] B. Rebbechi, C. Howard and C. Hansen, *Active control of gearbox vibration*, Proceedings of the Active control of Sound, Vibration conference, Fort Lauderdale, 1999, pp. 295-304.

[20] G. Pinte, S. Devos, B. Stallaert, W. Symens, J. Swevers and P. Sas, *A piezo-based bearing for the active structural acoustic control of rotating machinery*. Journal of Sound and Vibration, 329 (2010) 1235-1253.

[21] B. Stallaert, *Active structural acoustic source control of rotating machinery*, PhD thesis, KU Leuven University (2010).

[22] M. H. Chen, M. J. Brennan, *Active control of gear vibration using specially configured sensors and actuators*, Smart Materials and Structures 9(3) 2000 342-350.

[23] Y.H. Guan, M. Li, T.C. Lim and W.S. Shenpard Jr., *Comparative analysis of actuator concepts for active gear pair vibration control*, Journal of Sound and Vibration, 269 (1-2) (2004) 273-294.

[24] Y.H. Guan, T.C. Lim and W.S. Shenpard Jr., *Experimental study on active vibration control of a gearbox system*, Journal of Sound and Vibration, 282 (3-5) (2005) 713-733.

[25] M. Li, T.C. Lim, W.S. Shenpard Jr. Y.H. Guan, *Experimental active vibration control of gear mesh harmonics in a power recirculation gearbox system using a piezoelectric stack actuator*, Smart Materials and Structures, 14 (5) (2005) 917-927.

[26] M.J. Brennan, J. Garcia-Bonito, S.J. Elliott, A. David and R.J. Pinnington, *Experimental investigation of different actuator technologies for active vibration control*. Smart Materials and Structures (1999) 8 145-153.

[27] C.G. Diaz, *Active structural acoustic control smart panel with small scale proof mass actuators*, PhD thesis, University of Southampton, England (2007).

[28] A. Preumont, *Vibration Control of Active Structures*, London: Kluwer Academic. (2002).

[29] G. Zhao, W. Jacobs, B. Depraetere, N. Alujevic, G. Pinte and P. Sas, *Modal analysis of a piezo-based axisymmetric rotational vibration absorber*. Proceedings of 5th IOMAC International operational modal analysis conference (art.nr. Paper Id: No. 229).

[30] B. Widrow, J. Glover, J. McCool, J. Kaunitz, C. Williams, R. Hearn, J. Zeidler, E. Dong and R. Goodlin, *Adaptive noise cancelling: Principles and applications*. Proceedings of the IEEE (1975) 63 (12), 1692-1716.

[31] J. Glover, *Adaptive noise cancelling applied to sinusoidal interferences*. IEEE Transactions on Acoustics, Speech and Signal Processing (1977) 25(6), 484-491.

[32] D. Morgan and C. Sanford, *A control theory approach to the stability and transient analysis of the filtered-x lms adaptive notch filter*. IEEE transactions on Signal Processing (1992) 40(9), 2341-2346.

[33] S.M. Kuo and D.R. Morgan, *Active noise control: a tutorial review*, Proceedings of the IEEE (1999), Vol. 87(6), 943-973.

[34] N. Saito and T. Sone, *Influence of modelling error on noise reduction performance of active noise control systems using filtered-x lms algorithm*, Journal of the Acoustical Society of Japan (1998) 17(4), 195-202;